RESEARCH LETTER

# Correlating 3D morphology with molecular pathology: fibrotic remodelling in human lung biopsies


## ABSTRACT

Assessing alterations of the parenchymal architecture is essential in understanding fibrosing interstitial lung diseases. Here, we present a novel method to visualise fibrotic remodelling in human lungs and correlate morphological three-dimensional (3D) data with gene and protein expression in the very same sample. The key to our approach is a novel embedding resin that clears samples to full optical transparency and simultaneously allows 3D laser tomography and preparation of sections for histology, immunohistochemistry and RNA isolation. Correlating 3D laser tomography with molecular diagnostic techniques enables new insights into lung diseases. This approach has great potential to become an essential tool in pulmonary research.


"It takes more than cells to make a good lung", as Weibel[1] pointed out. The healthy lung is an efficient organ optimised towards a maximised surface and minimal diffusion barrier for gas exchange. The architecture that facilitates this organisation is based on thin elements of connective tissue providing stability and flexibility. Thus, understanding the three-dimensional (3D) architecture and parenchymal topography is essential to understanding lung function. This is not only true for the healthy lung, but even more so for pulmonary diseases where the 3D architecture is compromised, as, for example, in fibrosing interstitial lung diseases (ILD). Fibrotic changes are generally characterised by a spatially defined gain in tissue thickness due to accumulation of extracellular matrix, produced and modified by aggregates of activated myofibroblasts, as in ILD, for example, idiopathic pulmonary fibrosis or exogenous allergic alveolitis (EAA). Generally, the severity of disease is linked to the histopathological pattern and connectivity of fibrosis, which is responsible for the mechanical impairment of parenchymal dynamics.[2 3] In samples from patients with ILD in areas appearing unaffected in high-resolution CT (HRCT), Coxson and coworkers observed a considerable increase in the thickness of parenchymatous tissue by means of design-based stereology.[4] However, initial changes caused by the disease occur at a cellular level on a scale of microns, which cannot be depicted by HRCT scans and are therefore difficult to study in 3D, particularly in humans. Therefore, the goal of our study was to provide a method to visualise fibrotic remodelling of lung tissue in human lung biopsies and to demonstrate the correlation of morphological 3D data from individual fibrotic areas with gene expression analysis by miRNA or mRNA and immunohistochemistry.

Crucial for the analysis was the development of a novel embedding technique that combines different resins in order to clear the embedded samples to full optical transparency. With this novel technical approach the very same biopsy can be used for 3D tomography using scanning laser optical tomography (SLOT) and preparation of thin sections for histology, immunohistochemistry and RNA isolation after laser-assisted microdissection. Using SLOT the lung architecture can be visualised via endogenous absorption and fluorescence characteristics.[5]

Thereby, 3D imaging at a resolution of 10–12 μm was demonstrated in biopsies of a human lung explant from a patient suffering from end-stage EAA (figure 1). It was possible to identify areas of individual fibrotic remodelling and describe their morphological complexity through intensity,

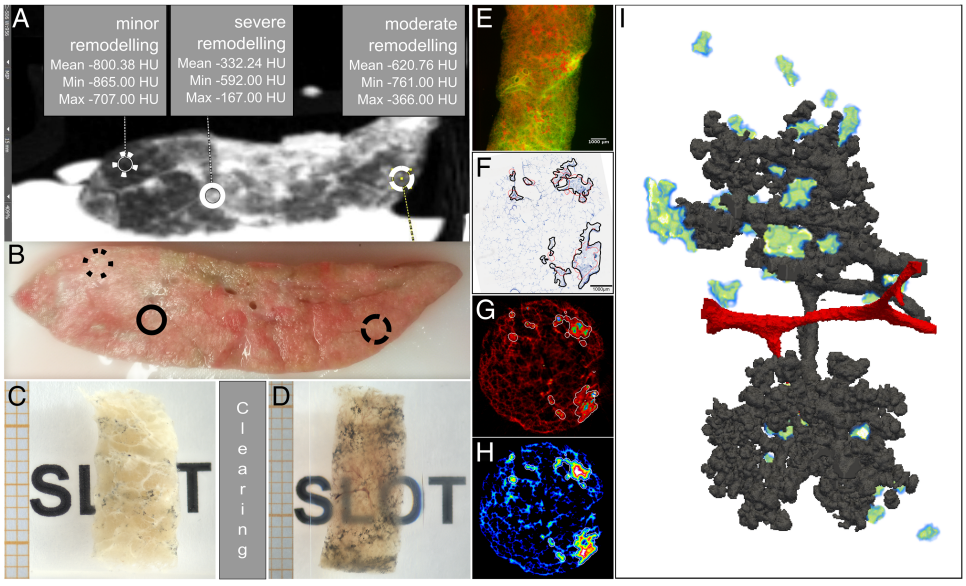


**Figure 1** Analysis of the fibrotic architecture in human lungs. Via high-resolution CT scanning of a fresh explanted lung, grading of remodelling intensity was performed (A). Based on this grading, samples were taken at indicated sites and used for solid-block clearing (B). For this, extracted human lung biopsies were fixated (C) and cleared in the resin mixture (D). Scanning laser optical tomography (SLOT) scanning: 800 projection images were taken at a wavelength of 532 nm. (E) shows one of these images combining autofluorescence (green) and absorption (red) signals. Subsequently, histopathological evaluation of the same sample was performed (F) and areas of fibrotic remodelling (black lines) were compared with areas identified as pathological via thickness analysis (red lines represent areas exceeding 300 μm in diameter). The distance cut-off model was based on a thickness analysis of the SLOT data sets (G) and correlated well with an increased absorption of the tissue (H). Segmentation model of airways (grey) and blood vessels (red) in the same sample showing fibrotic areas identified by the distance cut-off model from (F) to (H) in the three-dimensional context (I). For a virtual bronchoscopy through this model, as well as movies of the SLOT projection data sets, distance analysis and the animated segmentation model, see online supplementary movies S1–4.

thickness and branching analysis based on absorption data sets. These 3D results of individual fibrotic areas were then correlated with conventional histopathology and gene expression profiles. Finally, virtual endoscopy based on the absorption data set from small bronchi via terminal bronchioles into the alveoli is feasible. For study details, see online supplementary material.

In summary, optically cleared biopsies from human lung explants can be used to visualise the lung architecture in health and disease. By correlating high-resolution 3D information with histology, immunohistochemistry, mRNA and miRNA expression analysis, new insights into the different stages of (fibrotic) human lung diseases are possible. This diagnostic approach has great potential to become an essential tool in lung research.

**Manuela Kellner,[1,2] Judith Wehling,[2,3] Gregor Warnecke,[2,4] Marko Heidrich,[5] Nicole Izykowski,[2,3] Jens Vogel-Claussen,[2,6] Raoul-Amadeus Lorbeer,[5] Georgios Antonopoulos,[5] Sabina Janciauskiene,[2,7,8] Roman Grothausmann,[1,8] Lars Knudsen,[1,2] Tammo Ripken,[5] Heiko Meyer,[4,5] Hans Kreipe,[2,3] Matthias Ochs,[1,2,8] Danny Jonigk,[2,3] Mark Philipp Kühnel[1,2,8]**

[1]Institute of Functional and Applied Anatomy, Hannover Medical School, Hannover, Germany
[2]Biomedical Research in Endstage and Obstructive Lung Disease Hannover (BREATH), Member of the German Center for Lung Research (DZL), Hannover, Germany
[3]Institute for Pathology, Hannover Medical School, Hannover, Germany
[4]Department of Cardiothoracic, Transplantation and Vascular Surgery (HTTG), Hannover Medical School, Hannover, Germany
[5]Biomedical Optics Department, Laser Zentrum Hannover e.V., Hannover, Germany
[6]Department of Radiology, Hannover Medical School, Hannover, Germany
[7]Department of Experimental Pneumology, Hannover Medical School, Hannover, Germany
[8]REBIRTH Cluster of Excellence, Hannover Medical School, Hannover, Germany

**Correspondence to** Dr Mark Philipp Kühnel, Institute of Functional and Applied Anatomy, Hannover Medical School, Carl-Neuberg-Straße 1, Hannover 30625, Germany; kuehnel.mark@mh-hannover.de

**Acknowledgements** We would like to express our sincere gratitude to Susanne Kuhlmann and Regina Engelhardt for their excellent technical assistance, as well as Gareth Griffiths and Sheila Fryk for revising the text. Additionally, we would like to thank the developers and mailing list members of the open-source programmes Fiji (fiji.sc/Fiji), ITK-SNAP (itksnap.org/pmwiki/pmwiki.php), Paraview (paraview.org), ITK (itk.org), VTK (vtk.org), VMTK (vmtk.org), ImageMagick (imagemagick.org) and mencoder (mplayerhq.hu).

**Contributors** MK and JW contributed equally to this study and share first authorship. DJ and MPK contributed equally to this study and share senior authorship. MK, JW, DJ and MPK conceived and designed research; MK, JW, GW, MH, NI and MPK performed experiments; MK, JW, JV-C, HM, TR, DJ and MPK analysed data; MK, JW, DJ and MPK interpreted results of experiments; MK, JW, RG and MPK prepared figures; MK and RG prepared movies; MK, JW, DJ and MPK drafted manuscript; MK, JW, GW, MH, NI, JV-C, R-AL, GA, SJ, RG, LK, TR, HM, HK, MO, DJ and MPK edited and revised manuscript; MK, JW, GW, MH, NI, JV-C, R-AL, GA, SJ, RG, LK, TR, HM, HK, MO, DJ and MPK approved final version of manuscript.

**Funding** The REBIRTH Cluster of Excellence, German Center for Lung Research (DZL) and a habilitation grant from TUI and DFG (grant 30743/1).

**Competing interests** MH, MK, MPK, R-AL, DJ, NI and HM are involved in a pending patent application for the sample preparation procedure (DE 102014108642.2). Parts of the SLOT imaging technique are patented by the Laser Zentrum Hannover e.V. and are invented by MH, R-AL and HM (among others).

**Patient consent** Obtained.

**Ethics approval** Ethikvotum-Nr. 2050-2013 by the ethics committee of the Medical School of Hannover.

**Provenance and peer review** Not commissioned; externally peer reviewed.

▶ Additional material is published online only. To view please visit the journal online (http://dx.doi.org/10.1136/thoraxjnl-2015-207131).

**To cite** Kellner M, Wehling J, Warnecke G, *et al*. *Thorax* Published Online First: [*please include* Day Month Year] doi:10.1136/thoraxjnl-2015-207131

Received 31 March 2015
Revised 28 April 2015
Accepted 30 May 2015

*Thorax* 2015;**0**:1–2.
doi:10.1136/thoraxjnl-2015-207131

## REFERENCES

1 Weibel ER. It takes more than cells to make a good lung. *Am J Respir Crit Care Med* 2013;187:342–6.
2 Cool CD, Groshong SD, Rai PR, *et al*. Fibroblast foci are not discrete sites of lung injury or repair: the fibroblast reticulum. *Am J Respir Crit Care Med* 2006;174:654–8.
3 Bates JHT, Davis GS, Majumdar A, *et al*. Linking parenchymal disease progression to changes in lung mechanical function by percolation. *Am J Respir Crit Care Med* 2007;176:617–23.
4 Coxson HO, Hogg JC, Mayo JR, *et al*. Quantification of idiopathic pulmonary fibrosis using computed tomography and histology. *Am J Respir Crit Care Med* 1997;155:1649–56.
5 Kellner M, Heidrich M, Beigel R, *et al*. Imaging of the mouse lung with scanning laser optical tomography (SLOT). *J Appl Physiol* 2012;113:975–83.

# CORRELATING 3D MORPHOLOGY WITH MOLECULAR PATHOLOGY: FIBROTIC REMODELLING IN HUMAN LUNG BIOPSIES

Manuela Kellner[1,7*], Judith Wehling[2,7*], Gregor Warnecke[3,7], Marko Heidrich[4], Nicole Izykowski[2,7], Jens Vogel-Claussen[5,7], Raoul-Amadeus Lorbeer[4], Georgios C. Antonopoulos[4], Sabina Janciauskiene[6,7,8], Roman Grothausmann[1,8], Lars Knudsen[1,7], Tammo Ripken[4], Heiko Meyer[3,4], Hans Kreipe[2,7], Matthias Ochs[1,7,8], Danny Jonigk[2,7#] and Mark Philipp Kühnel[1,7,8#]

[1]Institute of Functional and Applied Anatomy, Hannover Medical School, Hannover, Germany.
[2]Institute for Pathology, Hannover Medical School, Hannover, Germany.
[3]Department of Cardiothoracic, Transplantation and Vascular Surgery (HTTG), Hannover Medical School, Hannover, Germany.
[4]Biomedical Optics Department, Laser Zentrum Hannover e.V., Hannover, Germany.
[5]Department of Radiology, Hannover Medical School, Hannover, Germany.
[6]Department of Experimental Pneumology, Hannover Medical School, Hannover, Germany.
[7]Biomedical Research in Endstage and Obstructive Lung Disease Hannover (BREATH), Member of the German Center for Lung Research (DZL), Hannover, Germany.
[8]REBIRTH Cluster of Excellence, Hannover Medical School, Hannover, Germany.

*These authors contributed equally to this study and share first authorship.
[#]These authors contributed equally to this study and share senior authorship.

Corresponding author - Mark Philipp Kühnel
Institute of Functional and Applied Anatomy, Hannover Medical School, Hannover, Germany
Carl-Neuberg-Straße 1, 30625 Hannover, Germany
E-mail: kuehnel.mark@mh-hannover.de
Telephone: 0511-532-3690, Fax: 0511-532-166741

Key words: clearing, Scanning Laser Optical Tomography, virtual endoscopy, 3D imaging

## MATERIAL AND METHODS

### Donor

The surgical lung explant from end-stage EAA was retrieved from the Institute of Pathology of Hannover Medical School with the approval of the Hannover Medical School Ethics Committee (No. 990-2011). The donor of the lung was a male patient, born in 1971, who was initially diagnosed with an EAA in 1984. From 2008 onward the patient had received medicinal therapy (Azathioprin 200mg 1-0-0, Acetylcystein 600mg 1-1-1, Prednisolon 22.5mg 1-0-0). In 2009 this therapy was supplemented with long-term oxygen therapy (16 h/d, 1.5-4 l/min). The last pretransplantation pulmonary function test showed a forced vital capacity (FVC) of only 23% and a forced expiratory volume in one second (FEV1) of 26% (amount of oxygen 3l/min). Based on clinical testing and a progressive decline in physical performance, the patient was listed for lung transplantation in September 2013. In October 2013, bilateral orthotopic lung transplantation was performed by the Department of Cardiothoracic, Transplantation and Vascular Surgery (HTTG) at Medical School Hannover (MHH) (age of patient at transplantation: 42 years, weight 79kg, height 184cm).

### Sample preparation

Samples were taken from an explanted right middle lung lobe from a patient suffering from EAA (Figure S1). Directly after explantation the lung was inflated with a standardized air pressure of 1.96hPa and high resolution computer tomography (HRCT) scanning was performed using a HRCT scanner (General Electric Lightspeed 16-Slice CT). Based on HRCT scan, severity and distribution of fibrotic changes were assessed by an experienced radiologist. After fixation samples were taken at representative areas with minor, moderate and severe remodelling using a custom-made stainless steel trepan of 6mm inner diameter.

**Clearing and SLOT microscopy**

For scanning laser optical tomography (SLOT)-imaging, the biopsies were dehydrated by 2 hour incubation steps in an increasing ethanol series (J.T.Baker, Center Valley, Philadelphia, USA) followed by an increasing xylene series (J.T.Baker). Thereafter, lung biopsies were transferred into an increasing resin mixture series (Norland Products Inc., Cranbury, New Jersey, USA) with an incubation time of 1 day per step. The refractive index n in the resin mixture monomer, which includes a combination of NOA68 and NOA71, was adjusted to n = 1.523 resulting in a refractory index of n = 1.556 in the polymer. Throughout the whole procedure lung samples were kept in a vacuum chamber to avoid the formation of gas bubbles. In order to avoid optical artifacts from the edges of the resin blocks during laser scanning, samples had to be placed in the middle of the resin pool. To this end, biopsies were mounted on spacer located in a disposable syringe filled with the resin mixture. After polymerizing for several minutes in UV-light at 4°C, the syringes were turned upside down, spacers were removed and polymerization was allowed to continue for a total of 24 hours. Following polymerization, the syringes were removed and the specimens were mounted on the rotation stage of the SLOT system.

To adapt the resin block to the external atmosphere during the measurement, a combination of two different silicone oils (High Vacuum Diffusion Pump Oil, Onlink Technologies GmbH, Hainburg, Germany and Indomet Penta, Gründau, Germany) were combined to achieve the same refractive index as for the specimen.

SLOT datasets were obtained in the transmission via the photodiode (PD) and fluorescence scan mode via the photomultiplier tube (PMT),[1, 2] at a wavelength of 532nm with a 570nm optical long pass filter,[3] (Figure S2). For one measurement the biopsies were rotated 360° and 800 projection images were taken by 1000 x 1000 pixels. Via a filtered back projection algorithm 3D reconstruction was performed to obtain volumetric data stacks,[4].

**Histology and immunohistochemistry**

Serial cut slides from every biopsy cylinder previously analysed by SLOT were stained by toluidine blue, Hematoxylin and Eosin (HE) and van Gieson's Stain (EvG) (Figure S3A-C) for conventional histopathological assessment of tissue remodelling and inflammation (e. g. presence of fibrosis, structural changes of the airways, remodelling of vascular structures, presence of leukocytes). Serial slides were also immunohistochemically stained for different markers of tissue remodelling (fibrosis, inflammation and smooth-muscle differentiation), following a standard ABC protocol (α-1-antitrypsin, CD34 and smooth muscle actin) (Figure S3D-F).

The immnuohistochemistry results observed in different compartments and histological patterns were scored semiquantitatively in at least three locations of the specimens, ranging from no apparent reaction (score 0), positivity in less than 30% (score 1), positivity in 30% and more / less than 60 % (score 2) and positivity in 60% of cells or more (score 3).

The staining intensity was assessed – where applicable – in the different entities / morphological compartments, ranging between no apparent reactivity, barely visible reactivity at high magnification (x400 weak), well recognizable reactivity at medium magnification (x100 intermediate) and high protein expression levels visible even at low magnification (x20 strong). For negative controls, the primary antibody was replaced by bovine serum albumin (BSA).

**Data visualisation and image analysis**

To quantify fibrotic changes different analytic approaches were applied (Figure S4). The grey value intensities in the PD datasets were visualised using a 6 shades colour lookup-table (LUT) (Figure S4B),[5]. In order to analyse the thickness profile the PD datasets were converted into binary datasets by an otsu threshold filter,[6] and 3D distance map,[7, 8] was computed. The resulting distance maps were colour coded with a 16 colour LUT (Figure S4C-

G). In addition, remodelled areas with a diameter of at least 300µm were extracted from the binary threshold datasets by a 3D opening filter,[9] to create a distance cut off model (Figure S4D red lines and Figure S5A-F). Thereafter 3D skeleton models of these regions were generated to analyse their complexity via branching analysis (Figure S5G-K). The 3D adaptive brush,[10] and the "snake tool" of ITKsnap,[8] was used for any manual segmentation. The virtual endoscopy was created with a combination of VMTK,[11], VTK,[12], python, Blender,[13], ImageMagick and mencoder.

**Laser-assisted microdissection and RNA extraction**

The embedded specimens were cut in sections of 3µm thickness and were mounted on a poly-L-lysin-coated membrane. After toluidine blue staining, the CellCut Plus system (Molecular Machines & Industries AG, Glattbrugg, Switzerland) was used for laser-assisted microdissection of target compartments: fibrotic parenchyma (FP) and normal parenchyma (NP) (excluding large vessels and small bronchi / bronchioli). Approximately 8500 cells were collected from each compartment and suspended in a proteinase K digestion buffer. After overnight digestion, mRNA was isolated using phenol-chloroform extraction and precipitation.

Complementary DNA (cDNA) was generated using the High Capacity cDNA Reverse Transcription Kit (Applied Biosystems, Foster City, CA, USA) and preamplified in 14 PCR cycles following the manufacturer's protocol. An amplicon size below 100bp was one of the criteria for target genes, enabling reliable gene expression analysis in fixed samples, essentially as previously described by us for formalin-fixed paraffin embedded (FFPE) tissues,[14, 15]. The microRNA analysis was performed as described previously,[16, 17] according to the manufacturer´s description (Applied Biosystems).

Gene expression analysis for mRNA (genes and abbreviations are listed in Table S1 and Figure S6) and microRNA was performed as double runs on a 7500HT Fast Real-Time PCR system and recorded by the 7500HT SDS 2.3 software (Applied Biosystems).

**Table S1**

| No. | target genes | synonym / full name |
|---|---|---|
| 1 | ACTA2 | α smooth muscle actin |
| 2 | CD14 | cluster of differentiation 14 |
| 3 | CD34 | cluster of differentiation 34 |
| 4 | COL3A1 | collagen, type III, alpha 1 |
| 5 | MMP2 | matrix metalloproteinase 2 |
| 6 | TIMP1 | tissue inhibitor of metalloproteinases 1 |
| 7 | POLR2A (reference gene) | RNA-polymerase 2 subunit A |

For negative controls, preamplificated cDNA was replaced by water. Cycle threshold (CT) values were calculated by normalization to the mean expression of the endogenous control gene POLR2A and were converted into $2^{-}\Delta CT$.

**RESULTS**

The overall approach to assess remodelling in lung explants is illustrated in Figure 1. A fixation protocol was established (Figure S1A) that inflates explanted lungs in a physiological state, as can be seen by HRCT (Figure S1B) before fixation. In order to allow sample preparation from remodelled areas of different severity, the HRCT tomogram was examined by an expert radiologist using a maximal intensity projection with a volume thickness of 1.5cm and a soft tissue reconstruction image kernel. Finally the slice indicated in red in Figure S1B and shown as a frontal view in Figure S1C, which contained areas with no visible remodelling (“minor” remodelling, approximately -800HU), moderately remodelled areas

(approximately -600HU) and severely remodelled areas (approximately -300HU) was prepared and sampled at indicated sites (Figure S1D). After embedding in the resin mixture and UV polymerization, biopsies became transparent and were usable for SLOT imaging (Figure S1E-G).

Images from the SLOT projection datasets scanned at 532nm are shown in Figure S2A-C and Movie S1. After reconstruction of projection images, the results allowed a specific identification of small airways and blood vessels, as well as the overall parenchymal architecture by using endogenous autofluorescence and absorption information as described in Kellner *et al.*,[7] for mouse lungs. A virtual endoscopy of the transmission tomogram is illustrating a path through the bronchus into the parenchyma (Movie S2). For a better understanding the topology of the airways and parenchyma is shown as a segmentation model (Figure S2D).

In order to identify areas of fibrotic remodelling and localise these areas within the 3D environment, samples were sectioned and used for histology. Areas showing fibrotic remodelling, identified by a qualified pathologist based on histology (Figure S3A-C) and immunohistochemistry (Figure S3D-F), are highlighted in Figure S4A (black line). These fibrotic areas correlated well with two parameters in corresponding slices from SLOT datasets: absorption intensity (Figure S4B) and tissue thickness (Figure S4C and D, Movie S3). Remodelled parenchyma in the absorption intensity model shows higher absorption labelled in green to blue compared to healthy tissue labelled in red, as indicated by an artificial colour set from Fiji.

To employ tissue thickness as a parameter to analyse lung samples, a distance map analysis was established (Figure S4C). The colour code represents the distance of tissue in µm at any point in the sample to the closest surface. Parenchyma consists of thin structures not exceeding 40µm in diameter. The connective tissue surrounding the veins and the bronchio-arterial bundle showed a maximum thickness of approximately 250µm. It can be seen that a

cut off value of 300µm (labels in yellow, red and white) can be used to discriminate between samples containing fibrotic remodelling ("moderate" and "severe") and healthy looking samples (control and "minor"). Figure S5A-D shows the visualisation of areas exceeding the distance cut off of 300µm. The samples differ in both an increase in number (Figure S5E) and an increase in volume (Figure S5F) of fibrotic remodelled areas. However, healthy control lungs cannot be discriminated from minor fibrotic samples. In addition, the complexity of these areas was visualised. For this, corresponding skeleton models were calculated and analysed (Figure S5G-K). Healthy control samples as well as minor fibrotic samples were characterized by very simple structures of the areas exceeding 300µm in diameter, since almost no branching was observed. In contrast, moderate fibrotic samples exhibit a higher complexity. Not only size but also the number of branches within these areas was significantly increased.

To allow the correlation of 3D pathomorphology data from individual fibrotic areas with molecular analysis, the resin embedding method was optimized towards mRNA and miRNA isolation, as well as histological and immunohistological staining. As a proof of principle, we demonstrate expression analysis after laser-assisted microdissection of a subset of target genes involved in fibrosis (Table 1 and Figure S6B and C). The areas from where mRNA was isolated are visualised in red and green in the 3D SLOT dataset (Figure S6A), virtual sections in Figure S6D and F as well as histological sections in Figure S6E and G respectively. For orientation the segmentation of a small airway opening in two acini is highlighted in blue Amplification products from the quantitative reverse transcriptase polymerase chain reaction (qRT-PCR) are shown quantitatively and qualitatively in Figure S6B and C. The complementary immunohistochemical stainings were observed to be compatible with the mRNA expression results.

In addition, a range of miRNA expressions of the lung tissue within the clearing resin block could be detected that are associated with vascular remodelling (miRNAs are listed in Table S2).

Table S2

| miRNA | relative expression | miRNA | relative expression |
|---|---|---|---|
| miRNA-17-5p | 1.29 | miRNA-92a | 2.33 |
| miRNA-18a | 0.21 | miRNA-126 | 1126.71 |
| miRNA-19a | 8.61 | miRNA-143 | 39.07 |
| miRNA-19b | 109.83 | miRNA-145 | 231.78 |
| miRNA-20a | 16.44 | miRNA-204 | 0.17 |
| miRNA-21 | 10.46 | | |

**DISCUSSION**

In our study, a correlative approach was established to visualise morphological changes of fibrotic remodelling in biopsies from human lungs. The goal was to develop a method which allows the analysis of lung fibrosis on a histological and molecular level in a three-dimensional (3D) context. The healthy lung is a highly efficient organ optimized towards a maximized surface and minimal diffusion distances for gas-exchange. The tensegrity architecture, which facilitates this organisation, is based on thin elements of connective tissue providing stability as well as flexibility. Understanding this architecture in health and disease is therefore of great importance. Fibrotic remodelling is associated with a multitude of pulmonary diseases. Generally, the severity of disease is linked to the connectivity of fibrosis, which is responsible for the mechanical impairment of parenchymal dynamics,[18, 19]. We hypothesize that different pathological interstitial changes can be studied even in end-stage lungs in the transition from healthy appearance to severely remodelled parenchyma. In

samples from idiopathic pulmonary fibrosis (IPF) patients from areas appearing unaffected in HRCT, Coxson and co-workers observed a considerable increase in the thickness of parenchymatous tissue by means of design-based stereology,[20]. However, initial changes of disease arise on a cellular level on a scale of microns, which is not depicted by HRCT scans and therefore difficult to study in 3D, particularly in humans. For this, a variety of novel methods have been established over the last few years. These range from detection of collagens via second harmonic generation microscopy (SHG),[21, 22] in lung fibrosis to highly sophisticated micro computed tomography (µCT) approaches in a variety of lung diseases,[23-25]. However, SHG microscopy is limited to small sample sizes and currently only applied in basic research due to costs and availability of SHG microscopes. µCT offers very high resolution and allows 3D analysis of relatively large biopsies. However, when used on chemically fixed samples, osmium or other metals are needed to get good µCT contrast and therefore samples are no longer usable for correlation of molecular approaches such as immunohistochemistry or RNA expression analysis. For that reason additional adjacent biopsies are usually taken and used for protein and / or RNA expression analysis and therefore correlation of 3D information and expression analysis is only indirect. In 2012 we therefore published the first description of SLOT on mouse lungs that had been cleared using methylsalicylate / benzylbenzoate (MSBB). However, the correlation of 3D SLOT images with histology was challenging due to deformation and shrinking of samples during the sample preparation procedure, since samples were first embedded in MSBB for 3D imaging and then rinsed with solvent until further embedding in Technovit 8100. Other methods developed over the last few years, e.g. Scale,[26], Clarity,[27, 28] or BABB,[29, 30] also suffer from the same deformation effects, especially when applied to a soft and deformable tissue like the lung. In all these studies correlation of 3D imaging with histology is never demonstrated. Our investigation strategy was designed to assess the pathogenic micro-architecture and correlate morphological findings with histology, immunohistochemistry and

gene expression within the very same biopsy. Since the shape of the lung in the air-inflated and post-fixed state is comparable, different states of disease can be identified and sampled, allowing a correlative approach.

Based on the HRCT scan and macroscopic appearance, we defined three magnitudes of fibrotic tissue remodelling: minor, moderate and severe. By embedding in the novel resin, samples were cleared, which is a prerequisite for analysis with light microscopical methods such as SLOT or light sheet microscopy.

The images generated by SLOT are based only on endogenous contrast features, such as absorption and autofluorescence. Bronchi and blood vessels can be reliably identified with their absorbance and autofluorescence and can be discriminated from small airways and alveoli. This is mostly due to the strong autofluorescence of collagen in these structures. Fibrotic areas showed high levels of collagen, but were more difficult to visualise by fluorescence due to the presence of newly formed blood vessels of irregular shape in these areas. These contained numerous erythrocytes, which blocked significant amounts of the fluorescent signal. However, the absorption channel combined the absorption of the blood vessels, collagen and cellular components of the fibrosis, and provided a reliable way to identify fibrotic changes (compare Figure S4A with S4B). Based on these tomograms segmentation models of lung topology can be made and correlated with areas of fibrotic remodelling (Figure S2D, S6A and Movie S4).

Another defining characteristic of fibrosis is an overall change in tissue thickness. Our data indicate that thickness analysis via 3D distance mapping is an appropriate way to identify individual fibrotic remodelling areas (compare Figure S4A and S4C). In the chronic form of EAA the focal changes, which are responsible for an increase in thickness, are characterized as regions of new blood vessels, fibroblasts, myofibroblasts and newly formed collagen,[31, 32]. In genuine IPF, these foci are thought to play a decisive role in the progression of disease, since the number of fibroblastic foci per lung biopsy correlated well with progressive

physiologic deterioration and shortened survival [33]. In order to analyse number, volume and complexity of the individual remodelled areas a cut off value of distance was used, which discriminates between different severities of remodelling and correlates well with histology (compare Figure S4A and S4D). The comparison of the percentage of tissue exceeding 300µm in diameter revealed significant differences between the respective biopsies (Figure S5A-D) with regard to number (Figure S5E) and tissue volume (Figure S5F). However, it should be noted that quantification of number, volume or shape of individual fibrotic areas is only possible if the fibrotic area is completely contained within the sample volume, and therefore the results shown at least for the "severe" sample are biased.

In addition, the number of fibrotic foci in 3D might not be the relevant parameter for the estimation of the severity of disease. Since the lung is composed of tubular airways organized by mostly dichotomous branching, surrounded by the interstitium, fibrotic foci are most likely a complex network, which only appears to be organized as individual foci in histological slices,[18]. In order to describe the complex network of the fibrotic areas the binary distance cut off models were transformed into skeletons. Here, the number of branches and the total branch lengths are indications of complex shapes. Our analysis showed that branching occurs in "moderate" and "severe" samples, but is almost non-existent in control samples and "minor" samples.

In order to show that individual analysis of 3D characteristics of fibrotic foci can be correlated with molecular analysis, we performed thin sectioning with the same biopsy that had been used for imaging before and successfully applied histology, immunohistochemistry and miRNA and mRNA extraction after laser-assisted microdissection to individual fibrotic areas. This can be regarded as a proof of concept using a variety of established markers of tissue remodelling.

Our novel embedding technique allows the identification of characteristic changes during fibrotic remodelling by SLOT and a subsequent preparation for histology,

immunohistochemistry and mRNA expression analysis within the very same sample in a correlative way. The visualisation of fibrotic areas as well as bronchi and blood vessels provides the possibility for a topological analysis. Therefore, our correlative approach encompassing changes from macroscopical down to the molecular level opens up a whole new perspective for diagnosis and research in a multitude of diseases.

**REFERENCE LIST**


1 Lorbeer R-A, Heidrich M, Lorbeer C, *et al.* Highly efficient 3D fluorescence microscopy with a scanning laser optical tomograph. *Opt Express* 2011;19(6):5419-5430.

2 Heidrich M, Kühnel MP, Kellner M, *et al.* 3D imaging of biofilms on implants by detection of scattered light with a scanning laser optical tomograph. *Biomed Opt Express* 2011;2(11):2982-2994.

3 Kellner M, Heidrich M, Beigel R, *et al.* Imaging of the mouse lung with scanning laser optical tomography (SLOT). *J Appl Physiol* 2012;113(6):975-983.

4 Kak A, Slaney M. Principles of Computed Tomographic Imaging. Piscataway NJ: *IEEE*; 1999.

5 Schindelin J, Arganda-Carreras I, Frise E. Fiji: an open-source platform for biological-image analysis. *Nat Meth* 2012;9(7):676-682.

6 Otsu N. A Threshold Selection Method from Gray-Level Histograms. *IEEE Trans Syst Man Cybern* 1979;9(1):62-66.

7 Maurer CR, Jr., Rensheng Q, Raghavan V. A linear time algorithm for computing exact Euclidean distance transforms of binary images in arbitrary dimensions. *IEEE Trans on Pattern Anal Mach Intell* 2003;25(2):265-270.

8 Johnson HJ, McCormick M, Luis I. The ITK Software Guide, Updated for ITK version 4.5., Kitware Inc;2013. Available from: http://itk.org/itkSoftwareGuide.pdf.

9 Lehmann G. Binary morphological closing and opening image filters. *Insight Journal* 2005:6. Available from: http://hdl.handle.net/1926/141.

10 Yushkevich PA, Piven J, Hazlett HC, *et al.* User-guided 3D active contour segmentation of anatomical structures: Significantly improved efficiency and reliability. *NeuroImage* 2006;31(3):1116-1128.

11 Antiga L, Piccinelli M, Botti L, *et al.* An image-based modeling framework for patient-specific computational hemodynamics. *Med Biol Eng Comput* 2008;46(11):1097-1112.

12 Schroeder W, Martin K, Lorensen B. The Visualization Toolkit: An Object-Oriented Approach to 3D Graphics. 4th ed. Kitware, Inc.; 2006.

13 Want C, Mielert F. vtkblender module. Uni Alberta 2008 July [cited 2014 July 31]; Available from: http://www.ualberta.ca/CNS/RESEARCH/Vis/VTKBlender/.

14 Jonigk D, Modde F, Bockmeyer CL, *et al.* Optimized RNA Extraction from Non-deparaffinized, Laser-Microdissected Material. In: *Murray GI, editor. Laser Capture Microdissection. 2 ed. Humana Press*; 2011. p. 67-75.

15 Bockmeyer CL, Maegel L, Janciauskiene S, *et al.* Plexiform vasculopathy of severe pulmonary arterial hypertension and microRNA. *J Heart Lung Transplant* 2012;31(7):764-772.

16 Liu B, Peng XC, Zheng XL, *et al.* MiR-126 restoration down-regulate VEGF and inhibit the growth of lung cancer cell lines in vitro and in vivo. *Lung Cancer* 2009;66(2):169-175.

17 Davis-Dusenbery BN, Chan MC, Reno KE, *et al.* Down-regulation of Kruppel-like factor 4 (KLF4) by microRNA.143/145 is critical for modulation of vascular smooth muscle cell phenotype by transforming growth factor-beta and bone morphogenetic protein 4. *J Biol Chem* 2011;286(32):28097-28110.

18 Cool CD, Groshong SD, Rai PR, *et al.* Fibroblast Foci Are Not Discrete Sites of Lung Injury or Repair. *Am J Respir Crit Care Med* 2006;174(6):654-658.

19 Bates JHT, Davis GS, Majumdar A, *et al.* Linking Parenchymal Disease Progression to Changes in Lung Mechanical Function by Percolation. *Am J Respir Crit Care Med* 2007;176(6):617-623.

20 Coxson HO, Hogg JC, Mayo JR, *et al.* Quantification of Idiopathic Pulmonary Fibrosis Using Computed Tomography and Histology. *Am J Respir Crit Care Med* 1997;155(5):1649-1656.

21 Pena A-M, Fabre A, Débarre D, *et al.* Three-Dimensional Investigation and Scoring of Extracellular Matrix Remodeling During Lung Fibrosis Using Multiphoton Microscopy. *Microsc Res Tech* 2007;70(2):162-170.

22 Abraham T, Hogg J. Extracellular matrix remodeling of lung alveolar walls in three dimensional space identified using second harmonic generation and multiphoton excitation fluorescence. *J Struct Biol* 2010;171(2):189-196.

23 Kampschulte M, Schneider CR, Litzlbauer HD, *et al.* Quantitative 3D Micro-CT Imaging of Human Lung Tissue. *RöFo* 2013;185(9):869-876.

24 McDonough JE, Yuan R, Suzuki M, *et al.* Small-Airway Obstruction and Emphysema in Chronic Obstructive Pulmonary Disease. *N Engl J Med* 2011;365(17):1567-1575.

25 Christenson SA, Brandsma C-A, Campbell JD, *et al.* miR-638 regulates gene expression networks associated with emphysematous lung destruction. *Genome Med* 2013;5(12):1-13.

26 Hama H, Kurokawa H, Kawano H, *et al.* Scale: a chemical approach for fluorescence imaging and reconstruction of transparent mouse brain. *Nat Neurosci* 2011;14(11):1481-1488.

27 Chung K, Deisseroth K. CLARITY for mapping the nervous system. *Nat Meth* 2013;10(6):508-513.

28 Tomer R, Ye L, Hsueh B, *et al.* Advanced CLARITY for rapid and high-resolution imaging of intact tissues. *Nat Protocols* 2014;9(7):1682-1697.

29 Dodt HU, Leischner U, Schierloh A, *et al.* Ultramicroscopy: three-dimensional visualization of neuronal networks in the whole mouse brain. *Nat Meth* 2007;4(4):331-336.

30 Becker K, Jährling N, Saghafi S, *et al.* Chemical Clearing and Dehydration of GFP Expressing Mouse Brains. *PLoS ONE* 2012;7(3):e33916.

31 Grunes D, Beasley MB. Hypersensitivity pneumonitis: a review and update of histologic findings. *J Clin Pathol* 2013;66(10):888-895.

32 Daniil ZD, Gilchrist FC, Nicholson AG, *et al.* A Histologic Pattern of Nonspecific Interstitial Pneumonia Is Associated with a Better Prognosis Than Usual Interstitial Pneumonia in Patients with Cryptogenic Fibrosing Alveolitis. *Am J Respir Crit Care Med* 1999;160(3):899-905.

33 Nicholson AG, Fulford LG, Colby TV, *et al.* The Relationship between Individual Histologic Features and Disease Progression in Idiopathic Pulmonary Fibrosis. *Am J Respir Crit Care Med* 2002;166(2):173-177.

**FIGURE LEGENDS**

Figure S1: **Sampling procedure.** Schematic illustration of lung explant inflation, High Resolution Computed Tomography (HRCT) and fixation by immersion (A). Localization of the sampling slice (thickness 1.5cm) in the HRCT-dataset (selected slice are labelled in red) (B). Grading of remodelling intensity in the slice visualised by a soft tissue analysis mode using a maximal intensity projection (C) and the corresponding lung slice (sampled areas are marked by black circles) (D). Extracted human lung biopsy after fixation (E) and clearing in the resin mixture (F). Through sectioning, three complementary analytic procedures (Scanning Laser Optical Tomography (SLOT), histology and mRNA expression) were combined for a comprehensive assessment of the development and progression of diffuse parenchymal lung disease (DPLD) (G).

Figure S2: **Projection datasets.** Transmission image (A) and fluorescence image (B). Overlay of the transmission mode in red and the fluorescence mode in green (C). Segmentation of conducting airways with the related acini (white), artery (red) and fibrotic changes (yellow) (D). Pulmonary blood vessel (*), conducting airways (●) and parenchyma (#). For more detail see Movie S1.

Figure S3: **Resin staining.** Histological sections of the "minor" biopsy with a staining of toluidine blue (A), Hematoxylin and Eosin (HE) (B), van Gieson's Stain (EvG) (C), as well as immunohistochemistry staining for α-1-antitrypsin (D), CD34 (E) and smooth muscle actin (F).

Figure S4: **Correlation of different analysis methods.** Histological section imaged by light microscopy with outlines of the pathological fibrotic findings (black lines) combined with an overlay of the distance cut off model (red lines) (A). Grey value intensity analysis (6 shades lookup-table (LUT) shows relative fluorescence intensity) (B) and distance analysis (16 colour LUT shows distance of tissue in µm at any point in the sample to the surface) (C) combined with the outlines of the distance cut off model marked in white. Otsu threshold of the reconstructed Scanning Laser Optical Tomography (SLOT) data stack combined with the distance cut off model (diameter 300µm) in white with red outlines (D).

Figure S5: **Visualisation of fibrotic remodelling by distance cut off models.** Rendered absorption tomograms with combined distance cut off models (red). Human biopsy from a healthy lung (A) and an extrinsic allergic alveolitis (EAA) explant showing minor (B), moderate (C) and severe fibrotic changes (D). Analysis results of number of fibroblastic foci per biopsy (E) and volume of fibrotic remodelled tissue in percent (F) of different stages of

remodelling. Quantification of branching as a measure for complexity (G) of the skeletons models (H-J).

Figure S6: **RNA analysis.** Rendered SLOT-dataset of a biopsy with “moderate” fibrotic remodelling. Two fibrotic foci are highlighted in green and red correspondingly (A) and the complementary gene expression profiles of the fibrotic parenchyma (FP) and the surrounding normal parenchyma (NP): selected target genes include ACTA2, CD14, CD34, COL3A1, MMP2 and TIMP1 (B). Gelelectrophoresis of qPCR products (C). Isolated areas (green (D) and red (F)) marked in SLOT slices and the corresponding histological sections (E and G). Insets show laser-assisted microdissection of selected areas.

Figure S1: Sampling procedure. Schematic illustration of lung explant inflation, High Resolution Computed Tomography (HRCT) and fixation by immersion (A). Localization of the sampling slice (thickness 1.5cm) in the HRCT-dataset (selected slice are labelled in red) (B). Grading of remodelling intensity in the slice visualised by a soft tissue analysis mode using a maximal intensity projection (C) and the corresponding lung slice (sampled areas are marked by black circles) (D). Extracted human lung biopsy after fixation (E) and clearing in the resin mixture (F). Through sectioning, three complementary analytic procedures (Scanning Laser Optical Tomography (SLOT), histology and mRNA expression) were combined for a comprehensive assessment of the development and progression of diffuse parenchymal lung disease (DPLD) (G).

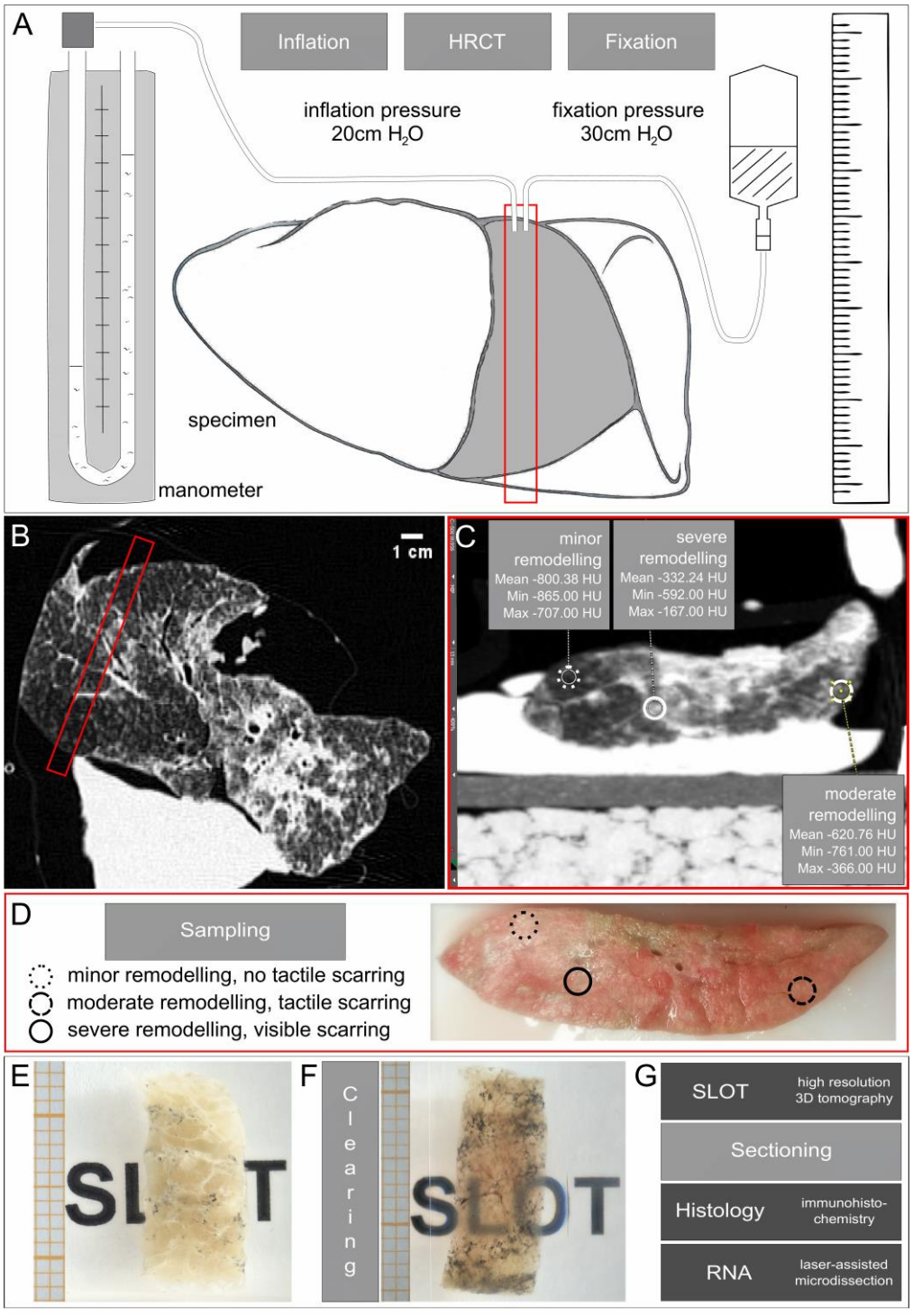

Figure S2: **Projection datasets.** Transmission image (A) and fluorescence image (B). Overlay of the transmission mode in red and the fluorescence mode in green (C). Segmentation of conducting airways with the related acini (white), artery (red) and fibrotic changes (yellow) (D). Pulmonary blood vessel (*), conducting airways (●) and parenchyma (#). For more detail see Movie S1.

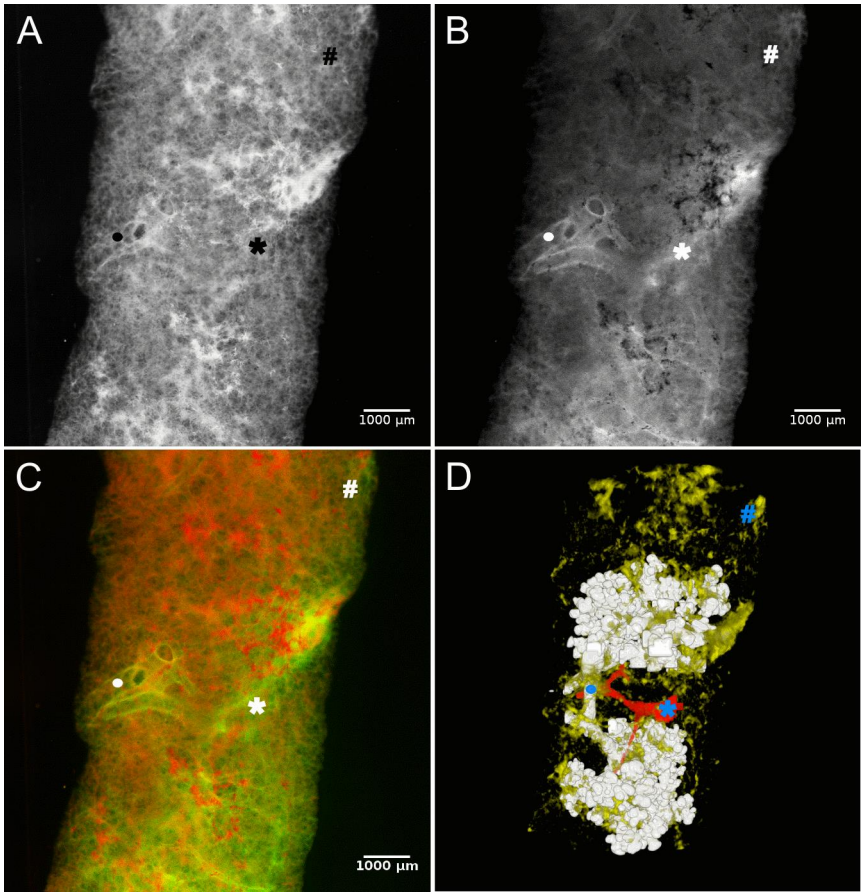

Figure S3: **Resin staining.** Histological sections of the “minor” biopsy with a staining of toluidine blue (A), Hematoxylin and Eosin (HE) (B), van Gieson's Stain (EvG) (C), as well as immunohistochemistry staining for α-1-antitrypsin (D), CD34 (E) and smooth muscle actin (F).

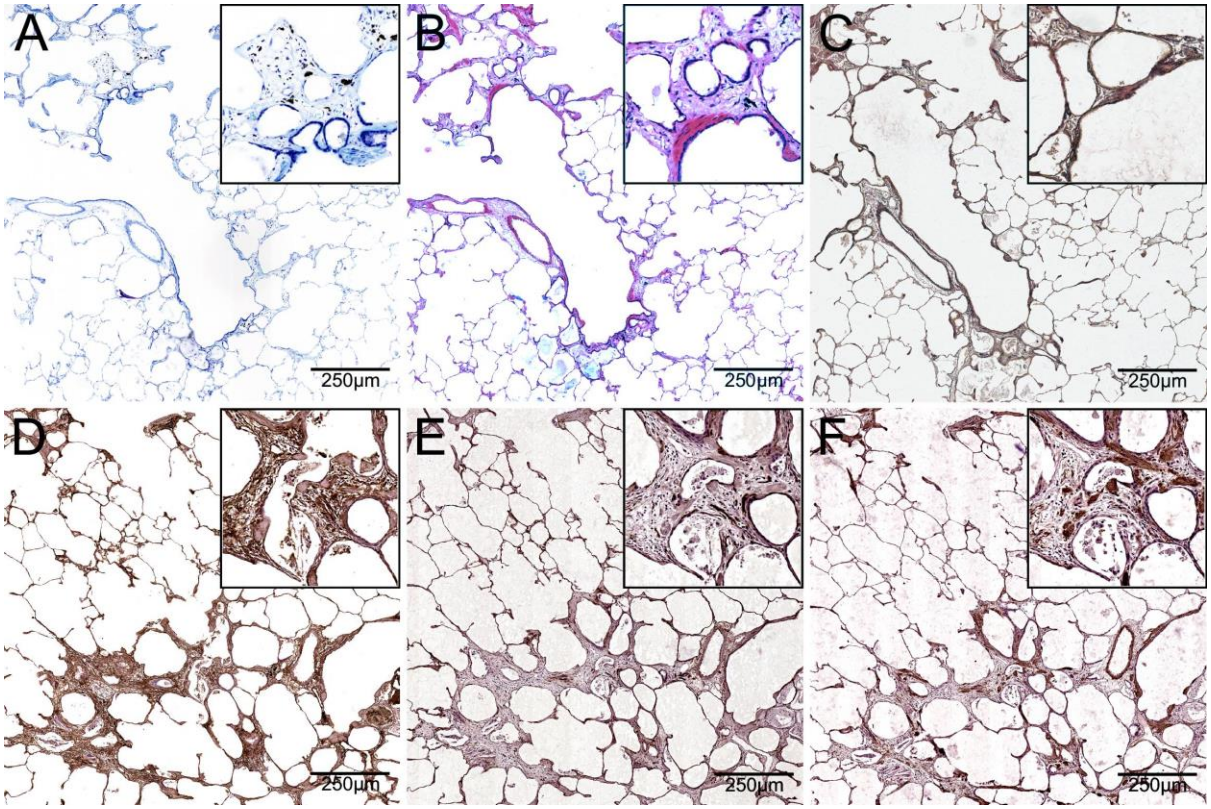

Figure S4: **Correlation of different analysis methods.** Histological section imaged by light microscopy with outlines of the pathological fibrotic findings (black lines) combined with an overlay of the distance cut off model (red lines) (A). Grey value intensity analysis (6 shades lookup-table (LUT) shows relative fluorescence intensity) (B) and distance analysis (16 colour LUT shows distance of tissue in µm at any point in the sample to the surface) (C) combined with the outlines of the distance cut off model marked in white. Otsu threshold of the reconstructed Scanning Laser Optical Tomography (SLOT) data stack combined with the distance cut off model (diameter 300µm) in white with red outlines (D).

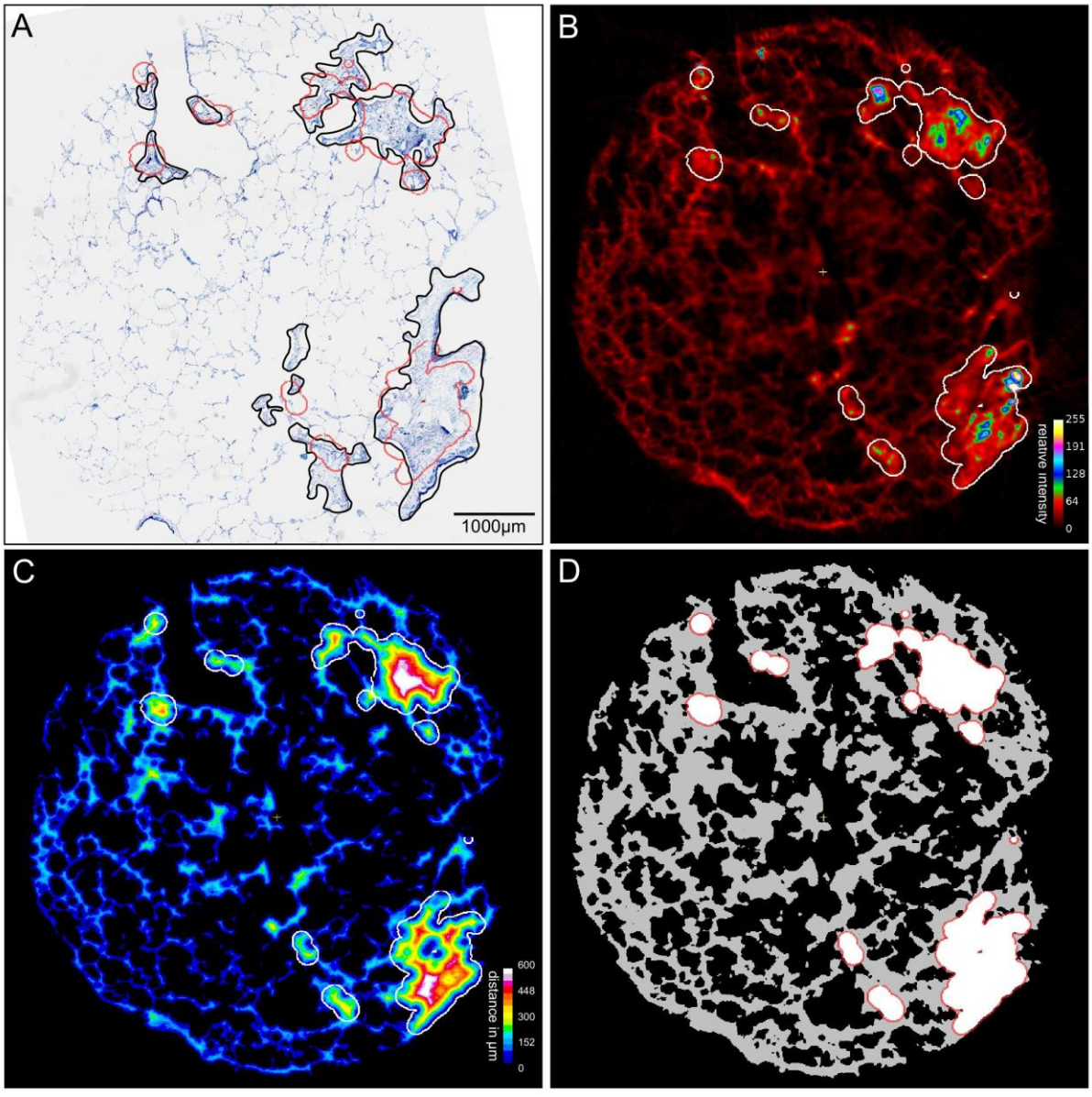

Figure S5: **Visualisation of fibrotic remodelling by distance cut off models.** Rendered absorption tomograms with combined distance cut off models (red). Human biopsy from a healthy lung (A) and an extrinsic allergic alveolitis (EAA) explant showing minor (B), moderate (C) and severe fibrotic changes (D). Analysis results of number of fibroblastic foci per biopsy (E) and volume of fibrotic remodelled tissue in percent (F) of different stages of remodelling. Quantification of branching as a measure for complexity (G) of the skeletons 1 models (H-J).

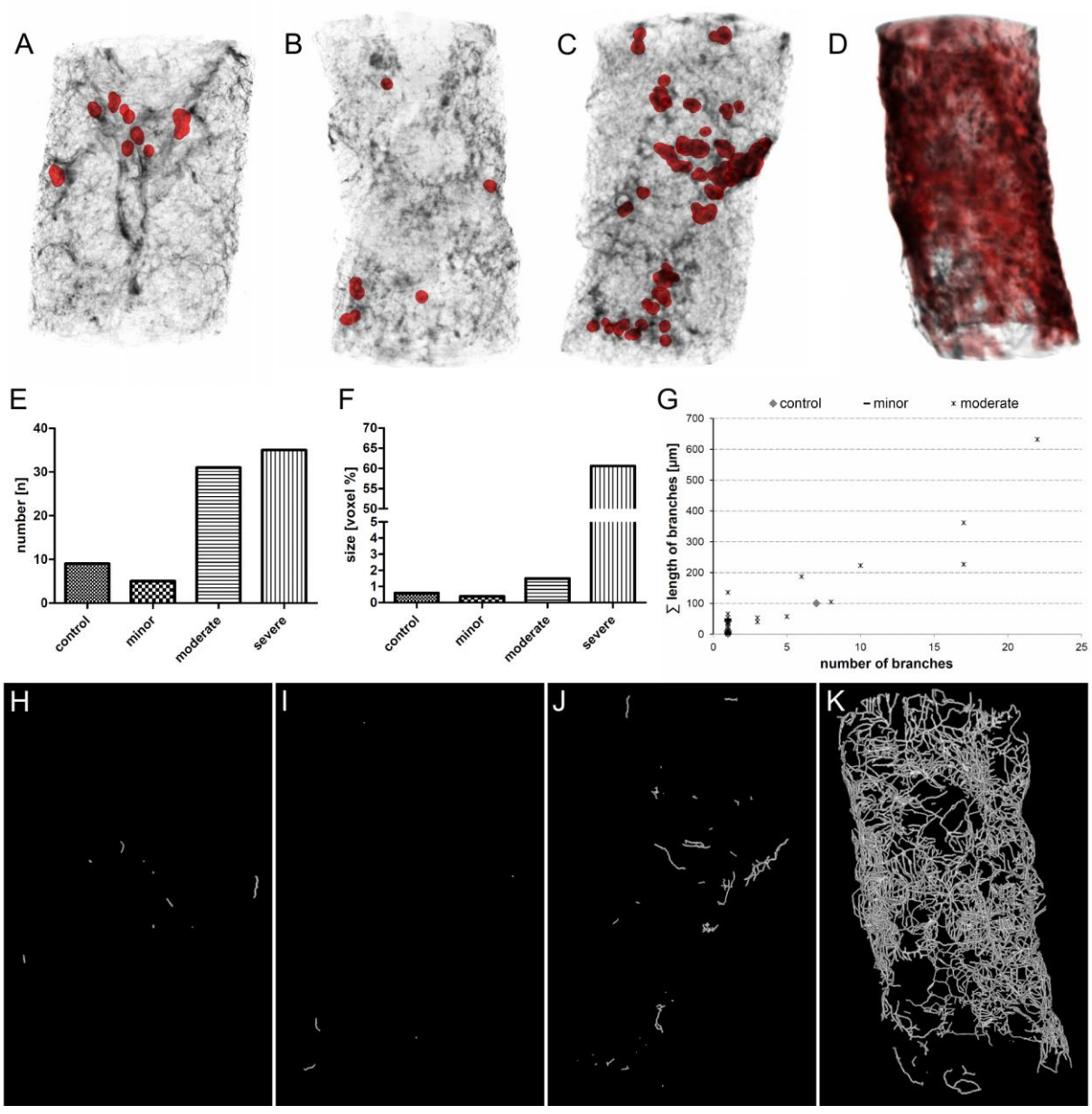

Figure S6: **RNA analysis.** Rendered SLOT-dataset of a biopsy with “moderate” fibrotic remodelling. Two fibrotic foci are highlighted in green and red correspondingly (A) and the complementary gene expression profiles of the fibrotic parenchyma (FP) and the surrounding normal parenchyma (NP): selected target genes include ACTA2, CD14, CD34, COL3A1, MMP2 and TIMP1 (B). Gelelectrophoresis of qPCR products (C). Isolated areas (green (D) and red (F)) marked in SLOT slices and the corresponding histological sections (E and G). Insets show laser-assisted microdissection of selected areas.

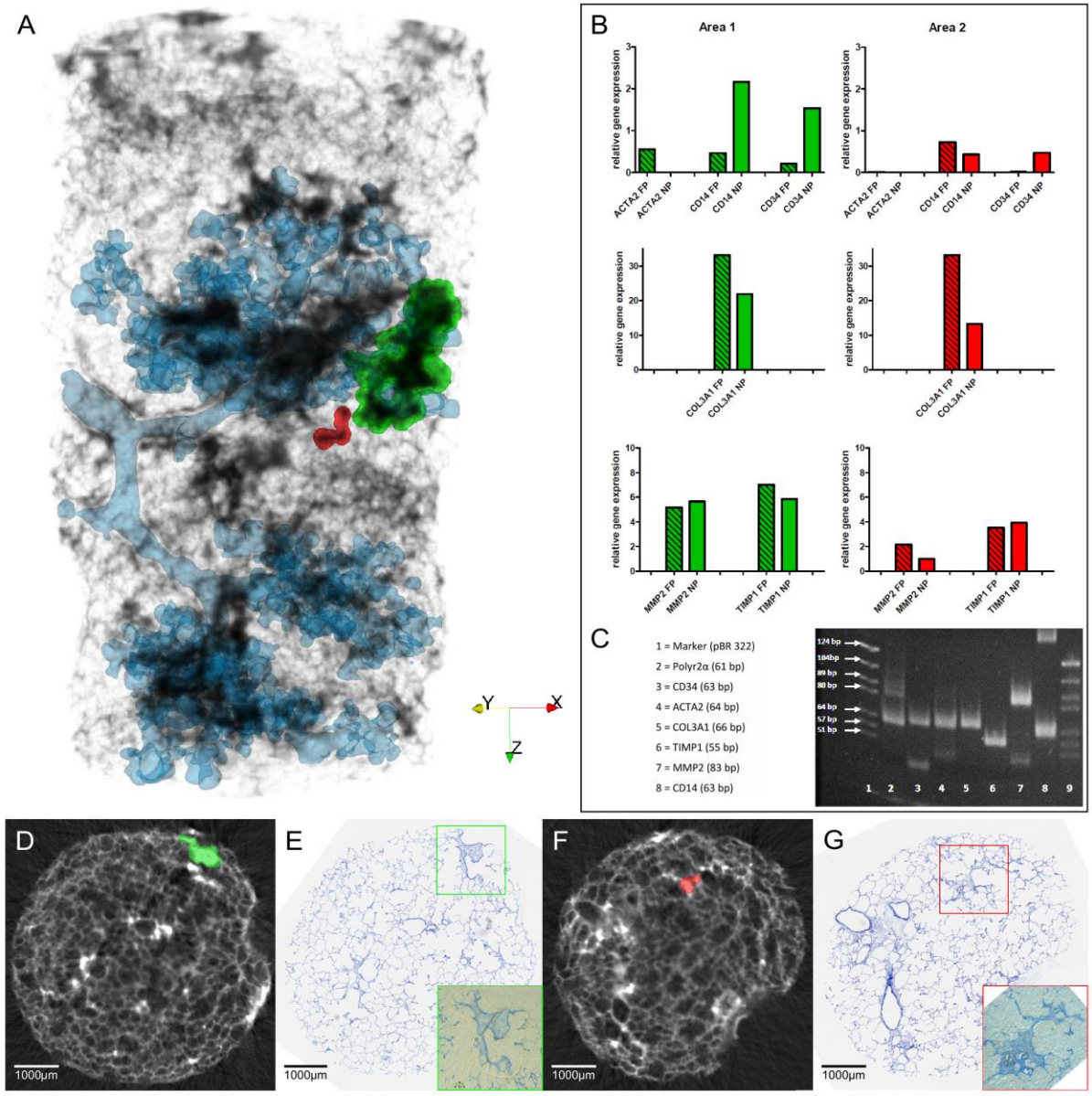

**MOVIE LEGENDS**

Movie S1: SLOT projection datasets of the “moderate” biopsy: Photodiode (PD) (A), photomultiplier tube (PMT) (B) and overlay of PD (in red) and PMT (in green) (C). Corresponding to Figure S2.

Movie S2: Virtual endoscopy of the “moderate” biopsy through a bronchus into the parenchyma. Inset shows an overview of the specimen topology together with the actual position.

Movie S3: Distance analysis of the healthy control biopsy (A), biopsy from an extrinsic allergic alveolitis (EAA) explant identified as minor (B), moderate (C) and severe fibrotic remodelling (D).

Movie S4: Segmentation of airways (grey) and blood vessels (red) in the “moderate” biopsycombined with distance analysis (blue) of the fibrotic areas (green) following by 300µm distance cut off model. Compare Figure S2D, and S5C.